International Journal of Minerals, Metallurgy and Materials
Volume 19, Number 12, Dec 2012, Page 1154
DOI: 10.1007/s12613-012-0685-0

Template-free synthesis of morphology- and size-controlled nano indium hydroxide

Chang-Yu Li and Shou-xin Liu

College of Material Science and Engineering, Northeast Forestry University, Harbin 150040, China
(Received: 20 February 2012; revised: 21 April 2012; accepted: 24 April 2012)

Abstract: Morphology- and size-controlled $In(OH)_3$ nanocrystals were synthesized via a novel, low-cost and low-temperature (70°C) route in the absence of any template and surfactant. The as-prepared products were characterized by X-ray diffraction (XRD), scanning electron microscopy (SEM), and high-resolution transmission electron microscopy (HRTEM) with selected area electron diffraction (SAED). The morphology and size of $In(OH)_3$ nanostructures can be controlled by adjusting the reaction conditions such as the reaction time, the concentration of the alkali, and the alkaline source. A possible mechanism for the evolution of the morphology- and size-controlled $In(OH)_3$ was proposed. In addition, the optical properties of the $In(OH)_3$ prepared by this method were studied by diffuse reflection spectra (DRS) and photoluminescence (PL) spectroscopy, and the results exhibit an obvious change of adsorption edges. The thermal behaviors of the as-prepared products were also explored by thermo-gravimetric (TG) and differential scanning calorimetry (DSC) measurements. According to the results of TG-DSC, the pure phase and uniformity of the In_2O_3 nanocube and nanorod can be obtained by annealing $In(OH)_3$ precursors directly at 300°C.

Keywords: indium hydroxide; synthesis; nanocrystals; nanostructures; morphology; optical properties

[*The project was financially supported by the Research Fund for the Doctoral Program of Higher Education of China (No.2110006210003) and the National Natural Science Foundation of China (No.31170545).*]

1. Introduction

In recent years, micro- and nano-crystals have received the increased interest because of their novel properties and potential applications [1-4]. Morphology- and size-controlled materials have been a research hotspot because the performances of materials depend on their morphology and size [5-7]. Therefore, the work on morphology- and size-controlled synthesis needs to be developed for more novel properties and applications of micro- and nano-materials. As an n-type wide-bandgap semiconductor, $In(OH)_3$ is a very promising material and has attracted increasing attention because of its extensive important applications such as catalysts [8-10], electrode materials [11], solar energy fields [12-13], and the precursors for In_2O_3, which is an important semiconductor material [14-16]. To date, much effort has been attempted to prepare $In(OH)_3$ nanostructures with different morphologies, such as nanocubes [8, 17-22], nanosheets [22], nanorods [22-24], nanospheres [19, 25], and nanoflowers [19, 26]. However, some of the above-mentioned methods need higher temperatures, and the others need templates, which complicate the synthetic processes. A facile and feasible method to prepare the morphology- and size-controlled $In(OH)_3$ is still a great challenge for materials scientists. Therefore, exploring new synthesis methods for controllable the morphologies and sizes of $In(OH)_3$ nanostructures will be significant to find new applications or to improve the existing performances.

Our previous work found that the nanorods of $In(OH)_3$ can be prepared via a one-step one-pot method [24]; however, in the further research, we could also obtain various $In(OH)_3$ nanostructures (single flake, rod, and cube) which

Corresponding author: Shou-xin Liu E-mail: liushouxin@126.com

we wanted, without any template or surfactant, and only adjusting the reaction parameters, such as the reaction time, the concentration of the alkali, and the alkaline source. A reasonable mechanism for the evolution of the morphology and size of $In(OH)_3$ nanocrystals was proposed. Through diffuse reflection spectra (DRS) and photoluminescence spectroscopy characterization, we can see that the as-prepared samples show excellent optical properties. In addition, we found that the pure phase and uniformity of the In_2O_3 nanocube and nanorod can be obtained by thermal decomposition of the $In(OH)_3$ precursors directly at 300°C

2. Experimental

2.1. Synthesis of $In(OH)_3$ samples

All chemicals used were analytic grade reagents and were used without further purification. $In(NO_3)_3{\cdot}4.5H_2O$ and urea were used as the starting materials. Deionized water was used as the solvent in all experiments.

In a typical synthesis (e.g., $In(OH)_3$-2), $In(NO_3)_3{\cdot}4.5H_2O$ (2 mmol) and urea (30 mmol) were dissolved in 140 mL of deionized water. Then the resulting mixture was transferred into a flask (250 mL capacity), heated at 70°C for 24 h and cooled to room temperature naturally. The obtained white precipitates were separated by centrifugation and washed several times with deionized water to remove residues and finally dried in air at 60°C. Other samples were prepared by a similar procedure to that for $In(OH)_3$-2 under different conditions in Table 1.

Table 1. Preparation of $In(OH)_3$ nanostructures under different conditions [a]

Sample name	$In(NO_3)_3{\cdot}4.5H_2O$ / mmol	Urea / mmol	NaOH / mmol	Ammonia / mmol	Time / h
$In(OH)_3$-1	2	15	0	0	24
$In(OH)_3$-2	2	30	0	0	24
$In(OH)_3$-3	2	120	0	0	24
$In(OH)_3$-4	1	30	0	0	24
$In(OH)_3$-5	2	0	30	0	24
$In(OH)_3$-6	2	0	0	30	24
$In(OH)_3$-7	2	30	0	0	6
$In(OH)_3$-8	2	30	0	0	12

Note: [a] all starting materials were dissolved in 140 mL of deionized water and the reaction temperature is 70°C.

2.2. Characterizations

X-ray diffraction (XRD) patterns of the prepared samples were recorded on a D/max-rB X-ray diffractometer with graphite-monochromatized Cu K_α radiation (λ=0.15418 nm), employing a scanning rate of 4°/min in the range from 15° to 90°. X-ray photoelectron spectroscopy (XPS) analysis was performed by a PHI5700 spectrometer and Al K_σ radiation (hv= 1486.6 eV); the binding energies were referenced to the C 1s line at 284.6 eV. The morphology and size of the as-prepared products were characterized by an environmental scanning electron microscope (ESEM, QUATA200). The high-resolution transmission electron microscope (HRTEM, Tecnai F30) with selected area electron diffraction (SAED) was employed to investigate the detailed nanostructures. Diffuse reflection spectra (DRS) of these samples were recorded on a TU-1900 UV-vis spectrometer equipped with an integral sphere using $BaSO_4$ as the reference. Photoluminescence (PL) emission spectra were measured using a Hitachi F-4500 fluorescence spectrophotometer. TG-DSC (a Pyris Diamond thermogravimetric/DSC apparatus) was used to analyze the thermal behavior of the as-synthesized samples with a heating rate of 10°C/min from room temperature to 600°C in air.

3. Results and discussion

3.1. XRD and XPS analysis

XRD patterns of the obtained nanocrystals are shown in Fig. 1, in which all the peaks can be indexed to a pure body centered cubic phase (bcc) (space group *Pn*3*m* (224)) of $In(OH)_3$ with the lattice constants of *a* (0.7980 nm for $In(OH)_3$-1, 0.7994 nm for $In(OH)_3$-2, 0.8040 nm for $In(OH)_3$-3,

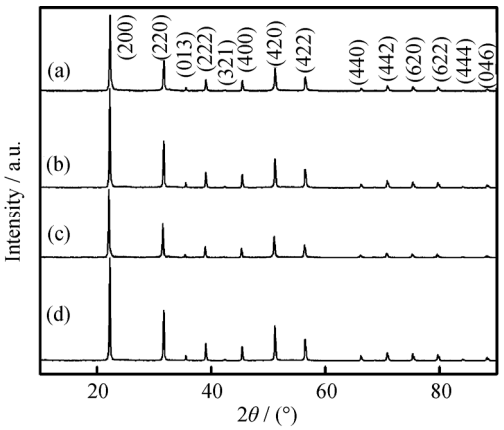

Fig. 1. XRD patterns of the as-prepared $In(OH)_3$ samples under different reaction conditions: (a) $In(OH)_3$-1, prepared in the solution of $In(NO_3)_3{\cdot}4.5H_2O$ (2 mmol) and urea (15 mmol) by reacting for 24 h at 70°C; (b) $In(OH)_3$-2 , prepared under the same conditions as $In(OH)_3$-1 except that urea is 30 mmol; (c) $In(OH)_3$-3, prepared under the same conditions as $In(OH)_3$-1 except that urea is 120 mmol; (d) $In(OH)_3$-4, prepared in the solution of $In(NO_3)_3{\cdot}4.5H_2O$ (1 mmol) and urea (30 mmol) by reacting for 24 h at 70°C.

and 0.7992 nm for $In(OH)_3$-4), which are very consistent with the literature value of *a* (0.7979 nm from JCPDS 85-1338); and it is also found from Fig. 1 that the relative intensity of the (220) face of the sample has been dramatically improved, indicating that the obtained $In(OH)_3$ nanocrystals might have a preferential growth direction [110].

The chemical composition of the $In(OH)_3$-2 was further characterized by X-ray photoelectron spectroscopy (XPS), and the obtained spectra are shown in Fig. 2. Peaks in Fig. 2(a) show that the surface of $In(OH)_3$-2 mainly consists of In and O. It is possible that the weak C 1s peak was caused by ineluctable carbon contamination in air. Further investigation based on the In $3d_{5/2}$ peak with the binding energy of 444.6 eV and the In Auger peak indicates that the surface of $In(OH)_3$-2 is composed of $In(OH)_3$ (Fig. 3(b)). The well symmetrical O 1s peak with the binding energy of 531.3 eV shown in Fig. 2(c) suggests that the oxygen species on the surface of $In(OH)_3$-2 is single, which also confirmed that $In(OH)_3$-2 is composed of $In(OH)_3$ only.

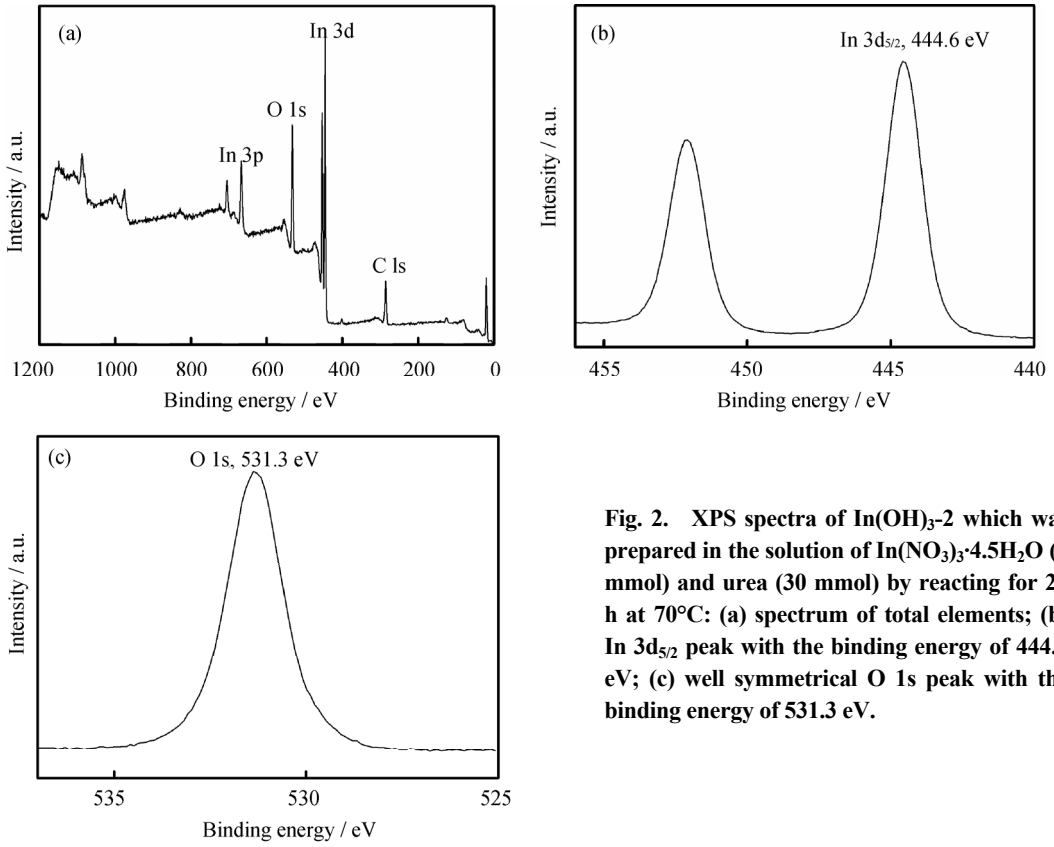

Fig. 2. XPS spectra of $In(OH)_3$-2 which was prepared in the solution of $In(NO_3)_3 \cdot 4.5H_2O$ (4 mmol) and urea (30 mmol) by reacting for 24 h at 70°C: (a) spectrum of total elements; (b) In $3d_{5/2}$ peak with the binding energy of 444.6 eV; (c) well symmetrical O 1s peak with the binding energy of 531.3 eV.

3.2. Morphology analysis

SEM images of the as-prepared samples from $In(OH)_3$-1 to $In(OH)_3$-4 are shown in Figs. 3(a)-3(d). As seen in Fig. 3, the morphologies of these obtained $In(OH)_3$ nanostructures are different because of differences in reaction conditions. In Fig. 3(a), we can see many $In(OH)_3$ nanocubes with the edge length ranging from 0.1 μm to 1.0 μm. All particles in $In(OH)_3$-2 shown in Fig. 3(b), obtained under the same condition as $In(OH)_3$-1 except that urea was 30 mmol, take on rod-like and cubic-like morphologies, the average edge lengths of rods or cubes are about 500 nm and 600 nm respectively, and many rod-like shape can be found in comparison to that in Fig. 3(a). Fig. 3(c) shows the morphologies of the $In(OH)_3$-3 prepared under the same condition as $In(OH)_3$-2 except that urea was 120 mmol. It is noted that $In(OH)_3$-3 is mainly rod-like, and the average edge length of rods is about 400 nm; moreover, $In(OH)_3$ nanocubes cannot be observed nearly. In Fig. 3(d) we can see the mixture of rod-like and cubic $In(OH)_3$ nanocrystals prepared under the same condition as $In(OH)_3$-2 except that $In(NO_3)_3 \cdot 4.5H_2O$ was 1 mmol, the nanorods is 200-400 nm in length and the nanocubes are 200-400 nm in edge length, and it can also be found that the size of particles decreases compared to the others. According to the SEM images, we can draw a conclusion that the morphology and size of $In(OH)_3$ can be controlled by adjusting the concentration of urea and $In(NO_3)_3 \cdot 4.5H_2O$.

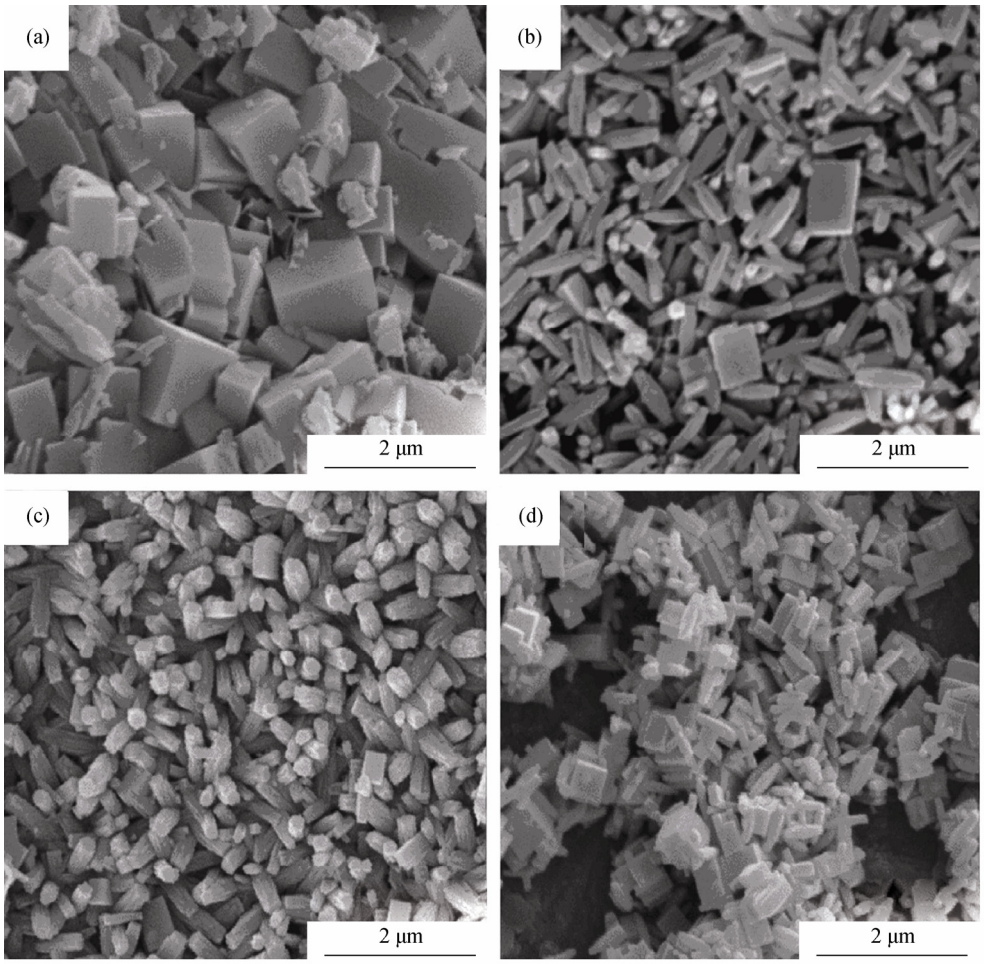

Fig. 3. SEM images of the as-synthesized $In(OH)_3$ nanostructures under different reaction conditions: (a) $In(OH)_3$-1; (b) $In(OH)_3$-2; (c) $In(OH)_3$-3; (d) $In(OH)_3$-4.

The structures of $In(OH)_3$ nanocrystals in $In(OH)_3$-2 were further characterized by HRTEM with SAED. As shown in Figs. 4(a) and 4(c), we clearly see that the nanorods and nanocubes were composed of a large number of individual nanoflakes. These $In(OH)_3$ nanoflakes self-assembled together and formed a closely packed nanocrystal rod or cube. The stacking structures of $In(OH)_3$-2 were further examined by HRTEM and shown in the insets of Figs. 4(b) and 4(d). The HRTEM images show the presence of perfectly crystallized particles. The fringe spacing (~0.288 nm) matches well with the separation between (220) lattice planes, implying the growth of the subunit is along the [110] direction, which is very consistent with the XRD results. The SAED pattern of many nanoparticles on the nanorod and nanocube are shown in the insets of Figs. 4(a) and 4(c). The clear diffraction spots can be observed in the SAED patterns, confirming the single-crystal nature of these particles, which also implies that all the particles on the rod and cube adopt high-orientation alignment.

3.3. Influencing factors

The nature of the precipitating agent has a great influence on the properties of the eventual products. In the control experiments, NaOH and $NH_3{\cdot}H_2O$ were used in place of urea, while other conditions were kept the same as that for preparing $In(OH)_3$-2. As shown in Fig. 5, when NaOH acts as the alkaline source, the resulting products were not only poor in crystallinity but also irregular in shape. When $NH_3{\cdot}H_2O$ was chosen as the alkaline source, only a few nanocubes can be seen in Fig. 5(b). From the above data, we can make a conclusion that the precipitating agent and the concentration of urea play important roles in the fabrication of the $In(OH)_3$ rod-like and cube-like morphologies. Because of the difficulty of releasing NH_3 from urea and the forming indium-urea complexes for the coordination between urea and In^{3+} [26], it is favorable for the subsequent growth of 1D and 3D nanostructures along the determined direction.

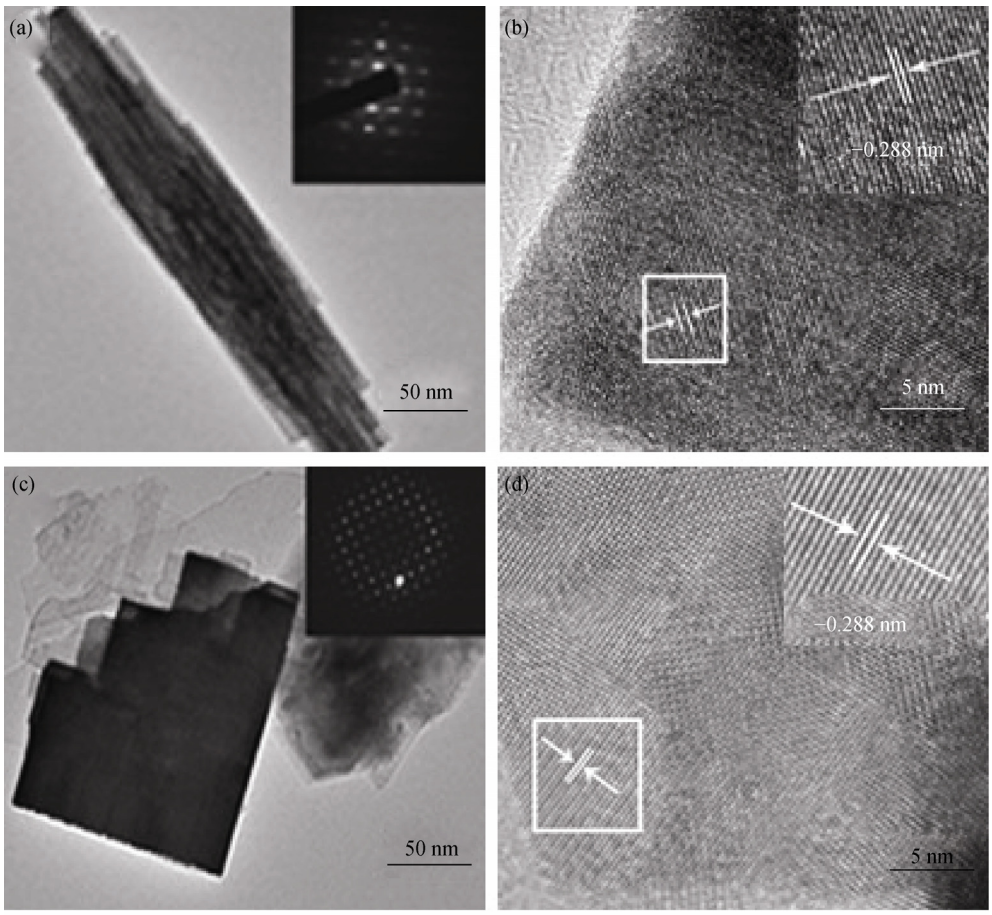

Fig. 4. TEM images of the different shapes of $In(OH)_3$-2 in Table 1: (a) $In(OH)_3$ rod and (c) $In(OH)_3$ cube (insets of (a) and (c) show the corresponding SAED patterns of sample 2); (b) and (d) the magnified TEM images of $In(OH)_3$-2 of (a) and (c) (insets of (b) and (d) show the corresponding HRTEM images of the framed region in (b) and (d) patterns).

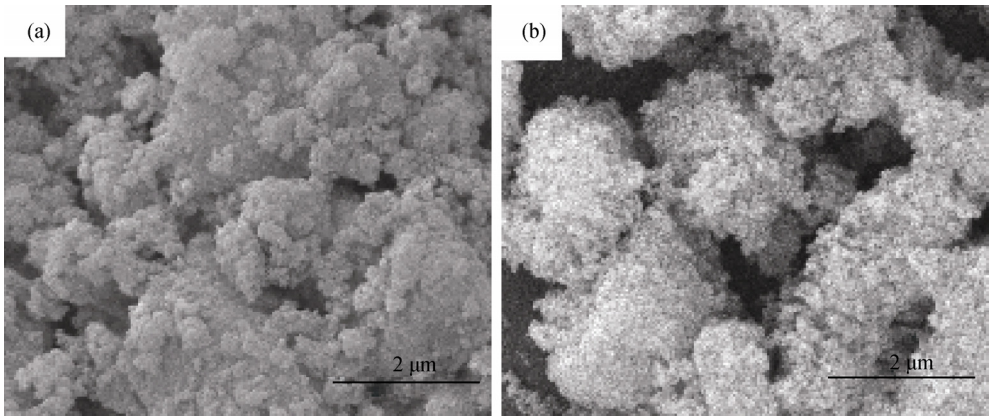

Fig. 5. SEM images of $In(OH)_3$ samples prepared by different precipitating agents as shown in Table 1: (a) $In(OH)_3$-5, prepared in the solution of $In(NO_3)_3{\cdot}4.5H_2O$ (2 mmol) and NaOH (30 mmol) by reacting for 24 h at 70°C; (b) $In(OH)_3$-6, prepared in the solution of $In(NO_3)_3{\cdot}4.5H_2O$ (2 mmol) and ammonia (30 mmol) by reacting for 24 h at 70°C.

3.4. Discussion of the formation mechanism

To further investigate the evolution process of the rod-like and cube-like $In(OH)_3$ nanostructures, time-dependent experiments were carried out, during which samples were collected at different reaction times after the reaction temperature reached 70ºC. At 6 h $In(OH)_3$-7 was collected, and many thin flakes can be seen from the TEM image in

Fig. 6(a). As shown in Fig. 6(b) ($In(OH)_3$-8 obtained at 12 h), the flake-like shape gets thicker than that of $In(OH)_3$-7; it is also found from Fig. 6(b) that there were some flakes starting to self-assemble into a cube-like and rod-like morphology. As the reaction proceeded for 24 h, a few single flakes can be seen from TEM images (in Fig. 6(c) and 6(d)) and most of them have transformed into nanorods and nanocubes. According to Figs. 3-5, we propose that the nanorods and nanocubes are self-assembled by the flakes and the concentration and ratio of reagents affect the nucleation and the self-assembly of thin flakes, as shown in Fig. 6. Many factors affect the evolution process of the flakes self-assembling into the rod-like and cube-like morphologies, such as electrostatic, dipolar fields associated with the aggregate, hydrophobic interactions, hydrogen bonds, crystal-face attraction and van der Waals forces. In this case, hydroxyl defects in the $In(OH)_3$ layer result in a positive charge of the layer, which can be confirmed by XPS results. The atom ratio of In to O is 1:2.72 (less than 1:3) according to the XPS result. Because of the existence of OH^- groups, electrostatic and hydrogen bonds might be the main driving forces for self-assembly, which followed Ostwald ripening kinetics. Such a process is similar to that in previous reports [27-28].

3.5. Optical properties analysis

The optical properties of $In(OH)_3$ nanocubes and nanorods were investigated by DRS spectra (Fig. 7(a)) and photoluminescence (PL) spectra (Fig. 7(b)). It can be observed from Fig. 7(a) that the adsorption edges of the samples change, indicating that the energy band changes.

$$\alpha E_p = K(E_p - E_g)^{1/2} \quad (1)$$

According to Eq. (1) for the semiconductor [14, 29], the values of band gap energy of these samples (from $In(OH)_3$-1 to $In(OH)_3$-4) can been be acquired and are 5, 5.06, 4.89 and 5.13 eV, respectively. These values are lower than those reported in Ref. [8], which is supposed that the oxygen vacancies (confirmed by the XPS result) of the $In(OH)_3$ prepared by this method decreased the band gap energy. The PL spectra of the as-prepared $In(OH)_3$ nanostructures are shown in Fig. 7(b). We find from Fig. 7(b) that all of the samples (from $In(OH)_3$-1 to $In(OH)_3$-4) have three PL emission peaks reported by previous studies [24, 30] from 470 to 750 nm locating at 491, 527.5 and 737.4 nm, respectively. Particularly, as shown in Fig. 7(b), it is noteworthy that the samples except for $In(OH)_3$-2 have luminescent wave bands with the emission peak centered at 610.5 nm (this emission peak is never reported), indicating that the as-prepared

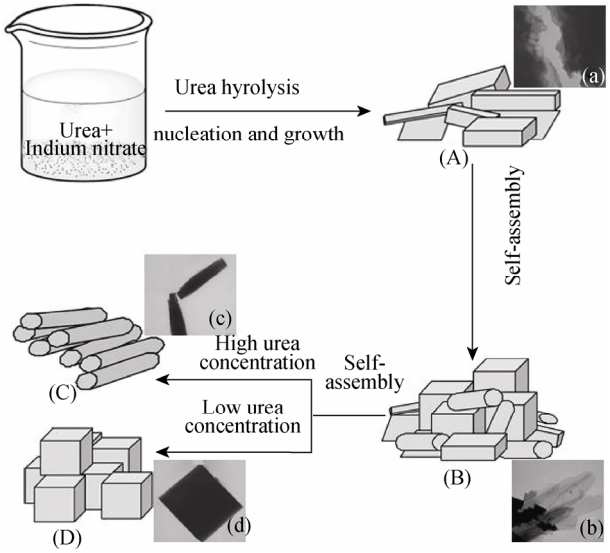

Fig. 6. Schematic representation of the growth process of rod-like and cube-like $In(OH)_3$ nanostructures. TEM images of (a), (b), (c), and (d) are corresponding to (A), (B), (C), and (D), respectively.

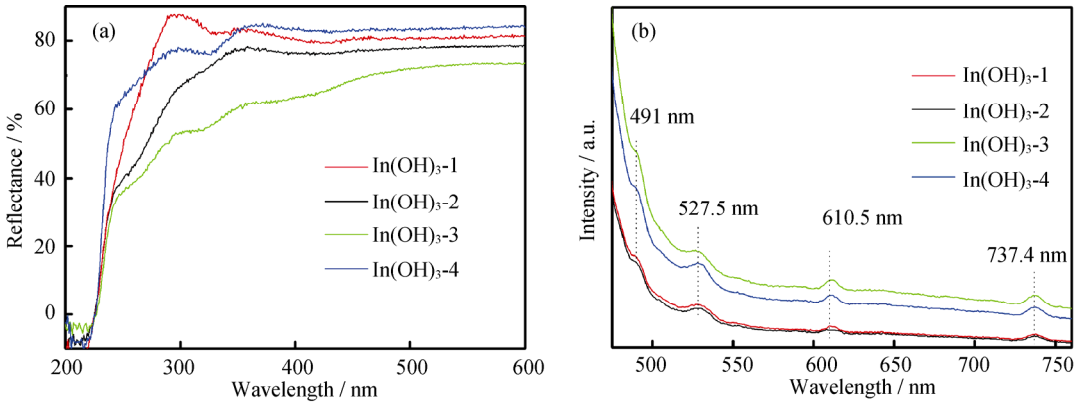

Fig. 7. Diffuse reflection spectra (a) and room temperature PL emission spectra (b) of the prepared $In(OH)_3$ nanostructures under the different conditions (excitation wavelength: 470 nm).

$In(OH)_3$ nanostructures possessed novel PL properties and will be interesting in the fabrication of optical material areas. Through the DRS and PL spectra we can see that the optical properties of the $In(OH)_3$ nanocrystals via this facile method have been improved to the same extent.

3.6. TG-DSC analysis

The thermal behavior of $In(OH)_3$-2 was investigated via TG-DSC measurement (Fig. 8). The TG curve (curve a) shows that the weight loss proceeds in three steps. A smooth loss (2%) in the range from 50 to 200°C is related to removing physical water evaporation from the $In(OH)_3$ sample. A large weight loss is observed from 200 to 400°C; the total weight loss of the process between 200 and 400°C is measured to be about 15.6%, which is close to the theoretical value (16.28%) calculated from the reaction of $2In(OH)_3 \longrightarrow In_2O_3 + 3H_2O$. The DSC curve (curve b) shows one maximum endothermic peak located at 286°C. The temperature range of the peak in the DSC curve fits well with that of weight loss in the TG curve, corresponding to endothermic behavior during the thermal decomposition-oxidation of $In(OH)_3$ to In_2O_3. A slight mass change from 400 to 600°C may be induced by disengaging of oxygen from bulk In_2O_3 crystal. We also explored the possibility of using $In(OH)_3$ as the precursor for synthesizing In_2O_3, which is a kind of useful wide band gap semiconductor oxides.

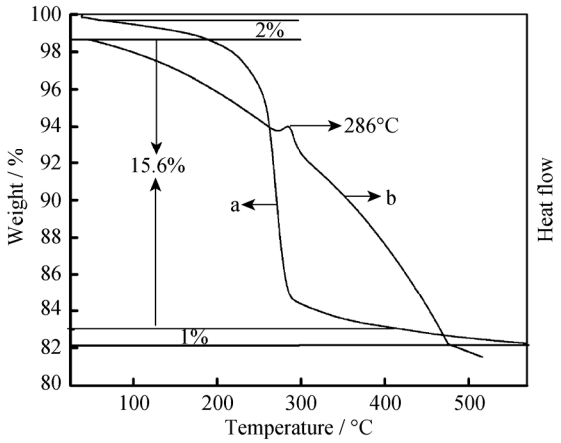

Fig. 8. TG-DSC curves of $In(OH)_3$-2, prepared in the solution of $In(NO_3)_3 \cdot 4.5H_2O$ (2 mmol) and urea (30 mmol) by reacting for 24 h at 70°C.

3.7. Phase and morphology analysis of In_2O_3

On the basis of TG and DSC results, we used 300°C to ensure the composition of In_2O_3. Fig. 9 shows the XRD pattern of the In_2O_3 powder prepared by thermal decomposition of the $In(OH)_3$ sample ($In(OH)_3$-2) at 300°C for 2 h. The diffraction peaks of In_2O_3 match well with cubic crystal In_2O_3 (JCPDS 06-0416), and no other characteristic peaks of impurities are observed, indicating that the pure phase of In_2O_3 can be obtained by annealing the $In(OH)_3$ precursors directly. The morphology of the as-prepared In_2O_3 was characterized by SEM in the inset of Fig. 9 and is similar to that of $In(OH)_3$-2.

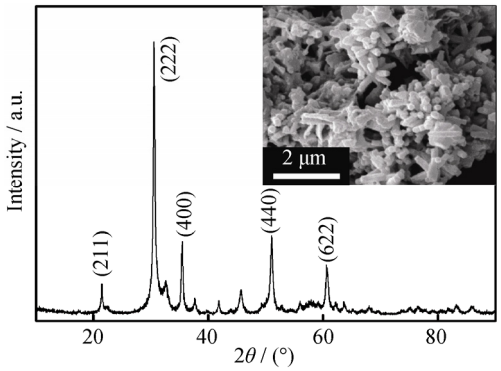

Fig. 9. XRD pattern of the as-prepared In_2O_3 powder by thermal decomposition of $In(OH)_3$ ($In(OH)_3$-2) at 300°C for 2 h. The inset is a SEM image of the In_2O_3 powder.

4. Conclusion

The morphology- and size-controlled $In(OH)_3$ nanostructures were successfully synthesized via a facile and low-cost method at 70°C in the absence of any templates or surfactants. Through adjusting the experimental conditions such as the reaction time, the concentration of the alkali and the alkaline source, the different sizes and morphologies of $In(OH)_3$ nanocrystals can be obtained. Among these experimental conditions, we found that the concentration of urea played a key role in the formation of controlling morphologies. The characterization results of DRS and PL indicate that the as-prepared morphology- and size-controlled $In(OH)_3$ nanostructures by this method have excellent optical properties, which will be interesting in the fabrication of novel optical material areas. Moreover, by thermal decomposition of the $In(OH)_3$ precursors directly at 300°C, the pure phase and uniformity of the In_2O_3 nanocube and nanorod can be obtained, which can enlarge the applications of the $In(OH)_3$ nanostructures.

References

[1] Z.H. Kang, E.B. Wang, L. Gao, S.Y. Lian, M. Jiang, C.W. Hu, and L. Xu, One-step water-assisted synthesis of high-quality carbon nanotubes directly from graphite, *J. Am. Chem. Soc*., 125(2003), p.13652.

[2] S.Y. Lian, E.B. Wang, Z.H. Kang, Y.P. Bai, L. Gao, L.M.

Jiang, C.W. Hu, and L. Xu, Synthesis of magnetite nanorods and porous hematite nanorods, *Solid State Commun*., 129(2004), No.8, p.485.

[3] M.H. Cao, X.Y. He, J. Chen, and C.W. Hu, Self-assembled nickel hydroxide three-dimensional nanostructures: a nanomaterial for alkaline rechargeable batteries, *Cryst. Growth Des*., 7(2007), No.1, p.170.

[4] P. Jiang, J.F. Bertone, and V.L. Colvin, A lost-wax approach to monodisperse colloids and their crystals, *Science*, 291(2001), p.453.

[5] L.X. Yang, Y.J. Zhu, H. Tong, Z.H. Liang, L. Li, and L. Zhang, Hydrothermal synthesis of nickel hydroxide nanostructures in mixed solvents of water and alcohol, *J. Solid State Chem*., 180(2007), No.7, p.2095.

[6] S.J. Park, S. Kim, S. Lee, Z.G. Khim, K. Char, and T. Hyeon, Synthesis and magnetic studies of uniform iron nanorods and nanospheres, *J. Am. Chem. Soc*., 122(2000), p.8581.

[7] D.L. Chen and L. Gao, A new and facile route to ultrafine nanowires, superthin flakes and uniform nanodisks of nickel hydroxide, *Chem. Phys. Lett*., 405(2005), p.159.

[8] T.J. Yan, X.X. Wang, J.L. Long, P. Liu, X.L. Fu, G.Y. Zhang, and X.Z. Fu, Urea-based hydrothermal growth, optical and photocatalytic properties of single-crystalline $In(OH)_3$ nanocubes, *J. Colloid Interface Sci*., 325(2008), No.2, p.425.

[9] T.J. Yan, J.L. Long, Y.S. Chen, X.X. Wang, D.Z. Li, and X.Z. Fu, Indium hydroxide: a highly active and low deactivated catalyst for photoinduced oxidation of benzene, *C. R. Chim.*, 11(2008), P.101.

[10] Z.B. Lei, G.J. Ma, M.Y. Liu, W.S. You, H.J. Yan, G.P. Wu, T. Takata, M. Hara, K. Domen, and C. Li, Sulfur substituted and zinc doped $In(OH)_3$: a new class of catalyst for photocatalytic H_2 production from water under visible light illumination, *J. Catal*., 237(2006), p.322.

[11] T. Ishida, K. Kuwabara, and K. Koumoto, Formation and characterization of indium hydroxide films, *J. Ceram. Soc. Jpn*., 106(1998), No.4, p.381.

[12] R. Bayón, C. Maffiotte, and J. Herrero, Chemical bath deposition of indium hydroxy sulphide thin films: process and XPS characterization, *Thin Solid Films*., 353(1999), No.1-2, p.100.

[13] R. Bayón and J. Herrero. Reaction mechanism and kinetics for the chemical bath deposition of $In(OH)_xS_y$, *Thin Solid Films*. 387(2001), No.1-2, p.111.

[14] S.K. Poznyak and A.I. Kulak, Characterization and photoelectrochemical properties of nanocrystalline In_2O_3 film electrodes, *Electrochim. Acta*, 45(2000), p.1595.

[15] J.Q. Xu, X.H. Wang, and J.N. Shen, Hydrothermal synthesis of In_2O_3 for detecting H_2S in air, *Sens. Actuator. B.*, 115(2006), p.642.

[16] Z.X. Cheng, X.B. Dong, Q.Y. Pan, J.C. Zhang, and X.W. Dong, Preparation and characterization of In_2O_3 nanorods, *Mater. Lett*., 60(2006), p.3137.

[17] Q. Tang, W.J. Zhou, W. Zhang, S.M. Ou, K. Jiang, W.C. Yu, and Y.T. Qian, Size-controllable growth of single crystal $In(OH)_3$ and In_2O_3 nanocubes, *Cryst. Growth Des*., 5(2005), No.1, p.147.

[18] H. Liang, Z.Y. Wang, N. Wang, Y. Li, and J. Yang, Hydrothermal synthesis of indium hydroxide nanocubes, *Mater. Lett*., 58(2004), p.2631.

[19] J. Du, M. Yang, S.N. Cha, D. Rhen, M.D. Kang, and J. Kang, Indium hydroxide and indium oxide nanospheres, nanoflowers, microcubes, and nanorods: synthesis and optical properties, *Cryst. Growth Des*., 8(2008), No.7, p.2313.

[20] X.F. Lu, T. Wang, X.Z. Zhang, A.G. Qiu, and D.L. Cui, Synthesis and characterization of $In(OH)_3$ nanocubes, *J. Phys. Conf. Ser.*, 188(2009), article No. 012010.

[21] F.V. Motta, R.C. Lima, A.P.A. Marques, M.S. Li, E.R. Leite, J.A. Varela, and E. Longo, Indium hydroxide nanocubes and microcubes obtained by microwave-assisted hydrothermal method, *J. Alloys Compd*., 497(2010), p.L25.

[22] J.H. Huang and L. Gao, Anisotropic growth of $In(OH)_3$ nanocubes to nanorods and nanosheets via a solution-based seed method, *Cryst. Growth Des*., 6(2006), No.6, p.1528.

[23] H.L. Zhu, K.H. Yao, Y.H. Wo, N.Y. Wang, and L.N. Wang, Hydrothermal synthesis of single crystalline $In(OH)_3$ nanorods and their characterization, *Semicond. Sci. Technol*., 19(2004), p.1020.

[24] C.Y. Li, S.Y. Lian, Y. Liu, S.X. Liu, and Z.H. Kang, Preparation and photoluminescence study of mesoporous indium hydroxide nanorods, *Mater. Res. Bull*., 45(2010), p.109.

[25] J. Yang, C.K. Lin, Z.L. Wang, and J. Lin, $In(OH)_3$ and In_2O_3 nanorod bundles and spheres: microemulsion-mediated hydrothermal synthesis and luminescence properties, *Inorg. Chem*., 45(2006), No.22, p.8973.

[26] H. Zhu, X.L. Wang, Z.J. Wang, C. Yang, F. Yang, and X.R. Yang, Self-assembled 3D microflowery $In(OH)_3$ architecture and its conversion to In_2O_3, *J. Phys. Chem. C*, 112(2008), No.39, p.15285.

[27] L.P. Xu, Y.S. Ding, C.H. Chen, L.L. Zhao, C. Rimkus, R. Joesten, and S.L. Suib, 3D flowerlike α-nickel hydroxide with enhanced electrochemical activity synthesized by microwave-assisted hydrothermal method, *Chem. Mater*., 20(2008), No.1, p.308.

[28] L.S. Zhong, J.S. Hu, H.P. Liang, A.M. Cao, W.G. Song, and L.J. Wan, Self-assembled 3D flowerlike iron oxide nanostructures and their application in water treatment, *Adv. Mater*., 18(2006), p.2426.

[29] Y.S. Luo, S.Q. Li, Q.F. Ren, J.P. Liu, L.L. Xing, Y. Wang, Y. Yu, Z.J. Jia, and J.L. Li, Facile synthesis of flowerlike Cu_2O nanoarchitectures by a solution phase route, *Cryst. Growth Des*., 7(2007) No.1, p. 87.

[30] Z. Shi, W. Wang, and Z.K. Zhang, Synthesis and characterization of indium hydroxide truncated polyhedral microcrystals, *Mater. Lett*., 62(2008), No.27, p.4293.